Published in final edited form as:
Invest Ophthalmol Vis Sci. 2005 June ; 46(6): 2012–2017.

Macular Segmentation with Optical Coherence Tomography

Hiroshi Ishikawa[1,2], **Daniel M. Stein**[1], **Gadi Wollstein**[1,2], **Siobahn Beaton**[1,2], **James G. Fujimoto**[3], and **Joel S. Schuman**[1,2]

1 *UPMC Eye Center, Department of Ophthalmology, University of Pittsburgh School of Medicine, Pittsburgh, Pennsylvania*

2 *New England Eye Center, Tufts-New England Medical Center, Tufts University School of Medicine, Boston, Massachusetts*

3 *Massachusetts Institute of Technology, Cambridge, Massachusetts*

Abstract

Purpose— To develop a software algorithm to perform automated segmentation of retinal layer structures on linear macular optical coherence tomography (StratusOCT; Carl Zeiss Meditec, Inc., Dublin, CA) scan images and to test its performance in discriminating normal from glaucomatous eyes in comparison with conventional circumpapillary nerve fiber layer (cpNFL) thickness measurement.

Methods— Four layer structures within the retina were defined: the macular nerve fiber layer (mNFL), the inner retinal complex (IRC; retinal ganglion cell [RGC] layer+inner plexiform and nuclear layers), outer plexiform layer (OPL), and outer retinal complex (ORC; outer nuclear layer +photoreceptor layer). Normal and glaucomatous eyes underwent fast macular map and fast NFL OCT scans. Linear macular images were analyzed using the developed algorithm, and the results were compared with the cpNFL thickness measurement.

Results— Forty-seven subjects (23 normal and 24 with glaucoma) were analyzed. mNFL, cpNFL, IRC, and the total retinal thicknesses were significantly greater in normal than in glaucomatous eyes ($P \leq 0.0002$; Wilcoxon), whereas OPL thickness did not show a significant difference ($P = 0.46$). ORC thickness was significantly greater in glaucomatous than normal eyes ($P = 0.035$). Areas under the receiver operator characteristic curve (AROCs) for discriminating normal from glaucomatous eyes were highest with mNFL+IRC (0.97) and lowest with OPL (0.56). AROCs for OPL and ORC were significantly smaller than those for mNFL, IRC, mNFL+IRC, and cpNFL ($P \leq 0.01$). AROCs for IRC, mNFL+IRC, and cpNFL were significantly larger than for retinal thickness ($P \leq 0.049$). Among the best-performing parameters (mNFL, IRC, mNFL+IRC, and cpNFL) there was no significant difference in AROCs ($P \geq 0.15$).

Conclusions— The newly developed macular segmentation algorithm described herein demonstrated its ability to quantify objectively the glaucomatous damage to RGCs and NFL and to discriminate between glaucomatous and normal eyes. Further algorithm refinement and improvements in resolution and image quality may yield a more powerful methodology for clinical glaucoma evaluation.

Clinical evaluation and management of glaucoma is largely dependent on functional testing and morphologic assessment of the optic nerve and the peripapillary nerve fiber layer (NFL).

Corresponding author: Hiroshi Ishikawa, UPMC Eye Center, Department of Ophthalmology, University of Pittsburgh School of Medicine, 203 Lothrop Street, Eye and Ear Institute, Room 841, Pittsburgh, PA 15213; ishikawah@upmc.edu.

Supported by National Eye Institute Grants EY13178, R01-EY11289, and P30-EY089898.

Disclosure: **H. Ishikawa**, None; **D.M. Stein**, None; **G. Wollstein**, None; **S. Beaton**, None; **J.G. Fujimoto**, Carl Zeiss Meditec (F); **J.S. Schuman**, Carl Zeiss Meditec (F)

The assessment can be accomplished with the use of visual field testing and stereobiomicroscopy of the optic nerve head and NFL. In the past decade, several ocular imaging modalities (scanning laser ophthalmoscopy, scanning laser polarimetry, and optical coherence tomography [OCT]) have been added to our array of diagnostic tools. However, these technologies are still in their infancy, and there is a need for improvement in scanning techniques and data analysis with these instruments.

Since Zeimer et al.[1] suggested the concept that macular thickness could be used as a measure of glaucoma, several studies have explored this idea by using emerging ocular imaging modalities, such as the retinal thickness analyzer (RTA)[2,3] and OCT.[4–8] The theory behind this concept is that assessment of macular thickness may be superior to circumpapillary nerve fiber layer (cpNFL) measurements, because retinal ganglion cell (RGC) bodies are 10 to 20 times the diameter of their axons and because the RGC layer is more than one cell thick in the macula.

Although the studies mentioned showed that visual function correlates significantly with cpNFL thickness and macular thickness, the cpNFL thickness measurement outperform the macular thickness in terms of magnitude of association with visual function.[4,7] This may be because the measured macular thickness represents the total retinal thickness. In this case retinal structures other than the RGC layer may confound the data so that the macular thickness measurement was not as sensitive as cpNFL thickness measurement.

The currently available commercial OCT unit (StratusOCT; Carl Zeiss Meditec, Inc., Dublin, CA) is the third generation of OCT technology, with a resolution of 8 to 10 μm and a scanning speed of approximately 400 Hz. With this high-resolution OCT, retinal layer structures can be distinguished in great detail. The purpose of this study was to develop a software algorithm to perform automated segmentation of retinal layer structures on linear macular OCT scan images and to test its performance in discriminating normal from glaucomatous eyes, in comparison with conventional cpNFL thickness measurement.

Materials and Methods

Algorithm Development

A software program featuring a new algorithm was developed within a software development environment (Visual Studio. Net, Microsoft, Redmond, WA). Raw data files of fast macular mapping OCT (StratusOCT Software, ver. 3.0; Carl Zeiss Meditec, Inc.) images (six radial linear scans with 6-mm scan length) were exported to an IBM-compatible computer. The new algorithm searched for borders of retinal layer structures on each sampling line (analogous to the A-scan line on ultrasonography) by applying an adaptive thresholding technique. A set of normal macular OCT images (learning set) was used to design the algorithm.

The summarized flow of the algorithm follows.

Preprocessing—Before segmentation, images were processed to yield better algorithm performance.

1. Aligned *z*-offset (starting location of the meaningful signal on each sampling line) by cross-correlation (shifting sampling lines so that the sum of the products of adjacent pixels is maximized; Fig. 1a).
2. Equalized the histogram of pixel intensity on each line by scaling the pixel intensities to the same minimum and maximum values.
3. Applied a modified mean filter (kernel size 7 × 5) to remove speckles (Fig. 1b).

Segmentation—The OCT A-scan profile consists of a series of peaks and valleys that represent various high and low tissue reflectivity of the retinal substructures (Fig. 2). Previous findings using ultra–high-resolution OCT aided in the definition of the borders of these substructures,[9,10] or retinal layers, as specific points on the A-scan profile, as follows:

1. The internal limiting membrane (ILM) was defined as the first highly reflective increase from the inner side on each sampling line. It was most often well demarcated, easily detected, and followed by a sector of high reflectivity. If not, the increase may have represented noise. The actual location of the border was determined by using an adaptive thresholding technique, where a cutoff threshold was calculated based on reflectivity histogram of each A-scan line. An integrity check with adjacent sampling lines was then performed to detect any disruption on the line of each of the detected structures by looking at the derivatives of the border location between the adjacent sampling lines. If the integrity check failed, the software automatically altered the internal parameters of the target peak (e.g., reflectivity threshold, peak width, and peak height) within a certain range and reran the seeking procedure. Another integrity check was then performed. If it failed, a quadratic regression line of the detected border locations was calculated in the vicinity of the target sampling line, and the closest eligible slope to this regression line was determined in the same fashion described earlier. The ability to discriminate noise from true tissue reflectivity was enhanced by this integrity check.
2. The retinal pigment epithelium (RPE) was sought on each sampling line by detecting two major peaks on each sampling line. The inner border of the second peak was then registered as the interface line of the inner and outer segments of the photoreceptors. A notch or gap close to this inner border within the complex was finally detected as the inner border of the RPE/choroid. The series of integrity checks and adjustment procedures described earlier were performed for every detected border line hereafter. The distance between the ILM and the inner border of the RPE/choroid was taken as the whole retinal thickness.
3. The deepest and widest “valley” within the retina was registered as the outer retinal complex (ORC), which consisted of outer nuclear layer and the inner and outer segments of the photoreceptors.
4. The innermost prominent peak between the ILM and the inner border of the ORC was designated the macular NFL (mNFL).
5. The outer most prominent peak before the ORC was designated the outer plexiform layer (OPL).
6. The residual area between the outer border of the mNFL and the inner border of the OPL was designated as inner retinal complex (IRC), which consisted of the RGC layer, inner plexiform layer, and inner nuclear layer.

Fig. 3 shows sample segmentation results superimposed on both original and filtered images. Note that these layer definitions are our presumption and may not reflect the actual anatomic structures.

Thickness Map Plotting—Thickness mapping was plotted as follows:

1. After thickness for each segment (mNFL, IRC, OPL, and ORC) on each image was calculated, the thicknesses of a set of six radial linear macular scan images were plotted on a Cartesian plane.
2. Values for points between actual measurements on the plane were calculated by polar interpolation.

Learning Set—A small group of subjects (5 normal eyes and 11 glaucomatous eyes) were used to subjectively assess the performance of the algorithm in proper border detection. These subjects were not used for the testing of the algorithm described in the next section.

Testing of the Algorithm

Subjects—Sixty-four subjects (27 normal and 37 with glaucoma) were scanned with a StratusOCT unit using the fast macular mapping and fast NFL scan modes (a set of three consecutive peripapillary circular scans 3.4 mm in diameter). Institutional Review Board (IRB) and Ethics Committee approval was obtained for the study, and all participants gave their informed consent to participate study. The study adhered to the principles of the Declaration of Helsinki.

All the participants had comprehensive ocular examination, reliable Swedish Interactive Thresholding Algorithm (SITA) standard 24-2 perimetry results (Carl Zeiss Meditec, Inc.), and OCT scanning of the macular and peripapillary regions at the same visit. All eyes had best corrected visual acuity of 20/40 or better, refractive error between −6.00 and +3.00 D, and no media opacities. Patients with diabetes, any medical condition that might affect visual field (VF) other than glaucoma, or treatment with medications that might affect retinal thickness were excluded from the study.

Normal subjects were healthy volunteers with normal ocular examination findings and VF glaucoma hemifield test (GHT) results within normal limits. All subjects with glaucoma had VF GHT results outside normal limits and a VF defect defined as one with fewer than 30% fixation losses, false-positive, or false-negative responses. They also had more than one of the following conditions: optic disc rim notching, cup asymmetry, large cupping (>0.7 vertical cup/disc ratio), NFL defect, or intraocular pressure >32 mm Hg. These glaucoma subjects had no history of ocular trauma or surgery other than glaucoma interventions or uncomplicated cataract extraction and no ocular diseases not attributed to glaucoma. One eye was randomly selected if both eyes qualified for the study.

Image Quality Control/Assessment—During acquisition, OCT scans had to demonstrate signal-to-noise ratio (SNR) ≥35 dB. Because SNR does not take into account all aspects of image quality (e.g., signal intensity distribution), we also used our previously presented quality index (QI) to further differentiate acceptable/unacceptable scans (Ishikawa H, et al. *IOVS* 2003;44:ARVO E-Abstract 3358; Ishikawa H, et al. *IOVS* 2004;45:ARVO E-Abstract 3317). QI was defined as a product of intensity ratio (IR) and tissue signal ratio (TSR), where IR was equivalent to SNR calculated from the logged raw data, and TSR was a ratio of the number of the pixels within a highly reflective area versus low reflective area. The cutoff of QI for poor-quality images on the OCT macular scan was 17.5 based on our unpublished data. Any subjects with a mean QI rating <17.5 for the six macular scans was excluded from the study.

Data and Statistical Analysis—All linear macular OCT images were analyzed by using the developed algorithm. cpNFL thickness was calculated by the OCT system software version 3.0 (Carl Zeiss Meditec, Inc.). Both algorithm outputs were subjectively evaluated by two experts (HI, DS) independently to detect algorithm errors. Criteria of algorithm error were obvious disruption of the detected border, and/or border wandering (detected border jumping to and from different anatomic structures) for >5% consecutive (i.e., an uninterrupted error) or 20% cumulative (i.e., adding up all errors amounts to 20% of the image width) of the entire image.

Thicknesses of four different retinal segments (mNFL, IRC, OPL, and ORC) were calculated on each linear macular image, and thickness maps were plotted on each set of fast macular

scans. Overall thicknesses of each segment were then calculated, incorporating interpolated point values.

Differences in thicknesses between normal and glaucomatous eyes were evaluated using the Wilcoxon test. The capability of discriminating normal from glaucomatous eyes was assessed according to the area under the receiver operator characteristic curve (AROC).

Results

Of the 64 subjects enrolled, 24 normal (mean SITA MD 0.09 ± 0.98 dB) and 24 glaucomatous eyes (mean SITA MD −6.87 ± 5.15) satisfied the OCT image quality criteria used in the study (75.0% [288/384 images] overall; 88.9% [144/162 images] in normal eyes, and 64.9% [144/222 images]) in glaucomatous eyes). One normal subject was excluded from the study because the algorithm failed to detect retinal borders on multiple images properly, based on the subjective experts' assessments.

Normal subjects were younger than subjects with glaucoma (52.1 ± 14.8 normal vs. 62.4 ± 14.5 glaucoma; $P = 0.02$, *t*-test).

Algorithm failure occurred more often with poor-quality (55.6%) than with good-quality (10.2%) images (Table 1). Expert assessment of algorithm failure showed high agreement between observers ($\kappa = 0.89$). The ILM border was the most reliable border, whereas the IRC border was the least reliable one (Table 2).

mNFL, IRC, and the total retinal thickness as well as cpNFL thickness were significantly thicker in normal than in glaucomatous eyes ($P \leq 0.0002$, Wilcoxon), whereas OPL thickness did not show significant difference ($P = 0.46$; Table 3, Fig. 4). ORC thickness was significantly thicker in glaucomatous than in normal eyes ($P = 0.035$). The power was 0.998 to detect a difference in mNFL, IRC, or mNFL+IRC measurements between glaucomatous and normal eyes with $\alpha = 0.05$. Age showed statistically significant linear correlation with all thickness parameters (Pearson correlation, all $P < 0.01$) except for ORC and OPL (both $P > 0.2$). QI also showed statistically significant linear correlation with all thickness parameters (all $P < 0.02$) except for OPL and total retinal thickness (both $P > 0.6$).

AROCs were highest with mNFL+IRC (0.97) and lowest with OPL (0.56; Table 4). AROCs for OPL and ORC were significantly smaller than ones for mNFL, IRC, mNFL+IRC, and cpNFL ($P \leq 0.01$). AROCs for IRC, mNFL+IRC, and cpNFL were significantly larger than that for total retinal thickness ($P \leq 0.049$). Among the top-performing parameters (mNFL, IRC, mNFL+IRC, and cpNFL) there was no significant difference in AROCs ($P \geq 0.15$).

The mNFL+IRC color thickness map plotted provided subjectively useful information (Fig. 5). In normal eyes, the thickness map clearly showed a C pattern, where nasal mNFL+IRC thickness was greater than temporal, corresponding to the papillomacular bundle (Fig. 5a). With glaucomatous eyes, loss of mNFL+IRC thickness was visualized corresponding to the visual field defect (Fig. 5b). In the case illustrated, mNFL+IRC thickness was thinner in the superior hemicircle around the macula, corresponding to the inferior visual field defect.

Discussion

Several studies have shown that macular thickness was reduced in glaucomatous compared with normal eyes.[3,5–8] The reduced macular thickness in glaucomatous eyes is attributed mainly to RGC and NFL loss.[11,12] The RGC and retinal nerve fiber layers contribute 30% to 35% of the retinal macular thickness, where the ganglion cells are known to be most concentrated.[3] This means that 65% to 70% of the macular thickness remains unchanged when

comparing normal and glaucomatous eyes. Therefore, to improve the discriminating power, the macular layers can be more finely divided so that only layers affected by glaucomatous damage are measured. However, with the 8- to 10-μm resolution available on the StratusOCT, we found that it was difficult to differentiate every single anatomic layer structure.

The use of the fast macular mapping mode, which limits the number of sampling lines (A-scans) per image to 128, may be controversial. The improved visualization of the retinal layers with StratusOCT in comparison with older-generation OCT units is not only due to its higher axial resolution (which is negligible) but also to its denser transverse sampling (up to 512 sampling lines per image), feasible because of the StratusOCT's 400 A-scan/s scan rate. Hence higher-density scans may theoretically have better retinal layer separation. However, the price for the higher-density scan, which is decreased scanning speed, should not be overlooked. Six images must be acquired for macular mapping, which makes the overall scanning time approximately 7.5 seconds or longer. StratusOCT does not provide a scan mode that performs six high-density scan in a rapid succession without stopping between each image acquisition. Therefore, scan registration (centering at the fovea) is less accurate than the fast macular mapping scan, which completes the scanning of six 128-sampling images in just under 2 seconds. We also found that, for segmentation purposes, the smoothed images (Fig. 1b) using 128, 256, and 512 A scans/image showed no significant difference in appearance or in segmentation algorithm performance (Ishikawa H, unpublished data, 2003). Therefore, we decided to use the most commonly used fast macular mapping scanning mode for this study.

To improve the stability of the algorithm, we combined several retinal layers so that detected borders showed minimum variability. We found that the outer borders of the mNFL, inner nuclear layer, and OPL were the most stable of all possible borders. Thus, four different segments (mNFL, IRC, OPL, and ORC) were detected by the algorithm.

Even after this simplification of macular segmentation, we experienced algorithm failure of at least one detected border in approximately 10% of the good-quality images. Although a higher failure rate in poor-quality images was expected, we were surprised to find that the algorithm failed on more than half of them. When considering the most common areas for failure, we found that the outer borders of the IRC and OPL were least reliable. This may have been because the IRC and OPL had less pixel intensity and blurrier borders than did the better-defined layers such as ILM, NFL, and RPE. Further refinement of the algorithm is required.

In the present population, 88.9% of the OCT images from normal and 64.9% from glaucoma eyes were successfully enrolled in the study as good-quality images. This implies that the diseased eyes were harder to get scanned in good quality.

All parameters but OPL showed significant differences between normal and glaucomatous eyes—a finding that agreed with previous histologic studies.[11,12] As expected, the total retinal thickness was greater in normal than in glaucomatous eyes, also in agreement with previous studies.[3,5–8] Because the normal and glaucoma groups were not age matched, these discrepancies could be due to age differences. We found statistically significant correlations between age and thickness parameters, except for OPL and ORC. However, based on the correlation analysis, the measured differences far exceeded the expected differences due to age (e.g., the measured difference in mNFL+IRC was approximately 30 μm, whereas the expected age-related difference was approximately 6.3 μm).

To our surprise, although the glaucoma discrimination power of the ORC was the second worst, the ORC was thicker in glaucomatous eyes than in normal ones. The ORC is a combination of the outer nuclear layer and photoreceptor layer. According to the current understanding of pathophysiology, these layers are thought not to be affected by glaucoma. A potential explanation of this finding is that our definition of ORC on the OCT A-scan profile was

inaccurate, perhaps encompassing more structural elements than expected. Further investigation is needed, especially in the correlation of histologic structures and OCT images.

Contrary to expectations, mNFL+IRC thickness was the best-performing macular segmentation parameter in the present study. Our expectation was that IRC thickness would be the best performer, because it was the closest to the RGC layer's thickness.

The biggest sources of instability were speckle noise and uneven tissue reflectivity across sampling lines within an image. There are two approaches to minimize these factors; higher resolution, and improved signal quality (signal-to-noise ratio). Of course, further sophistication of the algorithm by using better methods and procedures for preprocessing filtering and border detection may be another key to improving the overall performance of macular segmentation analysis.

Data from our group published by Guedes et al.[7] showed that the AROC of macular thickness (total retinal thickness) was 0.80 for discriminating normal from those with advanced glaucoma (mean MD, −12.0 dB). Although these data were based on the first-generation OCT unit, which provided lower resolution images than the StratusOCT we used in the present study, our results agree with these nearly perfectly. In other words, even with the higher-resolution images, total macular thickness showed quite similar discriminating power. A major reason for this is probably that macular thickness measurement did not take advantage of the improved resolution since the ILM and RPE were the most clearly identifiable layers, even on the lower resolution OCT images. One can argue this also in another way. As mentioned earlier, glaucomatous eyes may tend to have worse image quality than normal eyes, and all thickness parameters except for OPL and total retinal thickness showed significant correlations with QI. The combination of these facts may have yielded artifactiously higher sensitivities for mNFL +IRC and cpNFL, as well as a lower sensitivity for total retinal thickness.

Guedes et al.[7] and Wollstein et al.[4] reported that cpNFL was the best parameter among many different ocular imaging parameters in terms of glaucoma discrimination. In the present study, we found that mNFL, IRC, and mNFL+IRC performed at least as well as cpNFL and better than the whole retinal thickness. This was an unexpected finding, as the cpNFL had the following theoretical advantages over the mNFL: First, the OCT scanning pattern in the macula employs a spoke pattern configuration, whereas continuous circular scanning is used in the circumpapillary region. The spoke pattern may miss information between each linear scan. Whereas at the scan pattern's center the points are overlapping, at the farthest extreme, there is a 1.6-mm space between spokes. Second, since all retinal nerve fibers radiate toward the optic nerve head, circular scanning around the optic nerve head is capable of detecting damage in areas that are not covered in the macular scan (i.e., the representation of the 50% of the eye's ganglion cells that do not reside in the macula). Finally, injury to the RGC may not affect the detectable structure of the cell bodies early on, but could result in thinning of their axons. Further investigation is needed.

In conclusion, our newly developed automated algorithm for macular segmentation showed potential usefulness for objective quantification of glaucomatous macular RGC and NFL damage. Improved algorithm sophistication and in scan resolution and image quality may yield a powerful, novel method for clinical glaucoma evaluation.

References

1. Zeimer R, Shahidi M, Mori M, et al. A new method for rapid mapping of the retinal thickness at the posterior pole. Invest Ophthalmol Vis Sci 1996;37:1994–2001. [PubMed: 8814139]
2. Asrani S, Zeimer R, Goldberg MF, et al. Application of rapid scanning retinal thickness analysis in retinal diseases. Ophthalmology 1997;104:1145–1151. [PubMed: 9224468]

3. Zeimer R, Asrani S, Zou S, et al. Quantitative detection of glaucomatous damage at the posterior pole by retinal thickness mapping. A pilot study. Ophthalmology 1998;105:224–231. [PubMed: 9479279]

4. Wollstein G, Schuman JS, Price LL, et al. Optical coherence tomography (OCT) macular and peripapillary retinal nerve fiber layer measurements and automated visual fields. Am J Ophthalmol 2004;138:218–225. [PubMed: 15289130]

5. Giovannini A, Amato G, Mariotti C. The macular thickness and volume in glaucoma: an analysis in normal and glaucomatous eyes using OCT. Acta Ophthalmol Scand Suppl 2002;236:34–36. [PubMed: 12390129]

6. Greenfield DS, Bagga H, Knighton RW. Macular thickness changes in glaucomatous optic neuropathy detected using optical coherence tomography. Arch Ophthalmol 2003;121:41–46. [PubMed: 12523883]

7. Guedes V, Schuman JS, Hertzmark E, et al. Optical coherence tomography measurement of macular and nerve fiber layer thickness in normal and glaucomatous human eyes. Ophthalmology 2003;110:177–189. [PubMed: 12511364]

8. Lederer DE, Schuman JS, Hertzmark E, et al. Analysis of macular volume in normal and glaucomatous eyes using optical coherence tomography. Am J Ophthalmol 2003;135:838–843. [PubMed: 12788124]

9. Drexler W, Morgner U, Ghanta RK, Kartner FX, Schuman JS, Fujimoto JG. Ultrahigh-resolution ophthalmic optical coherence tomography (published correction appears in *Nat Med*. 2001;7:636). Nat Med 2001;7:502–507. [PubMed: 11283681]

10. Fujimoto JG. Optical coherence tomography for ultrahigh resolution in vivo imaging. Nat Biotechnol 2003;21:1361–1367. [PubMed: 14595364]

11. Frishman LJ, Shen FF, Du L, et al. The scotopic electroretinogram of macaque after retinal ganglion cell loss from experimental glaucoma. Invest Ophthalmol Vis Sci 1996;37:125–141. [PubMed: 8550316]

12. Glovinsky Y, Quigley HA, Pease ME. Foveal ganglion cell loss is size dependent in experimental glaucoma. Invest Ophthalmol Vis Sci 1993;34:395–400. [PubMed: 8440594]

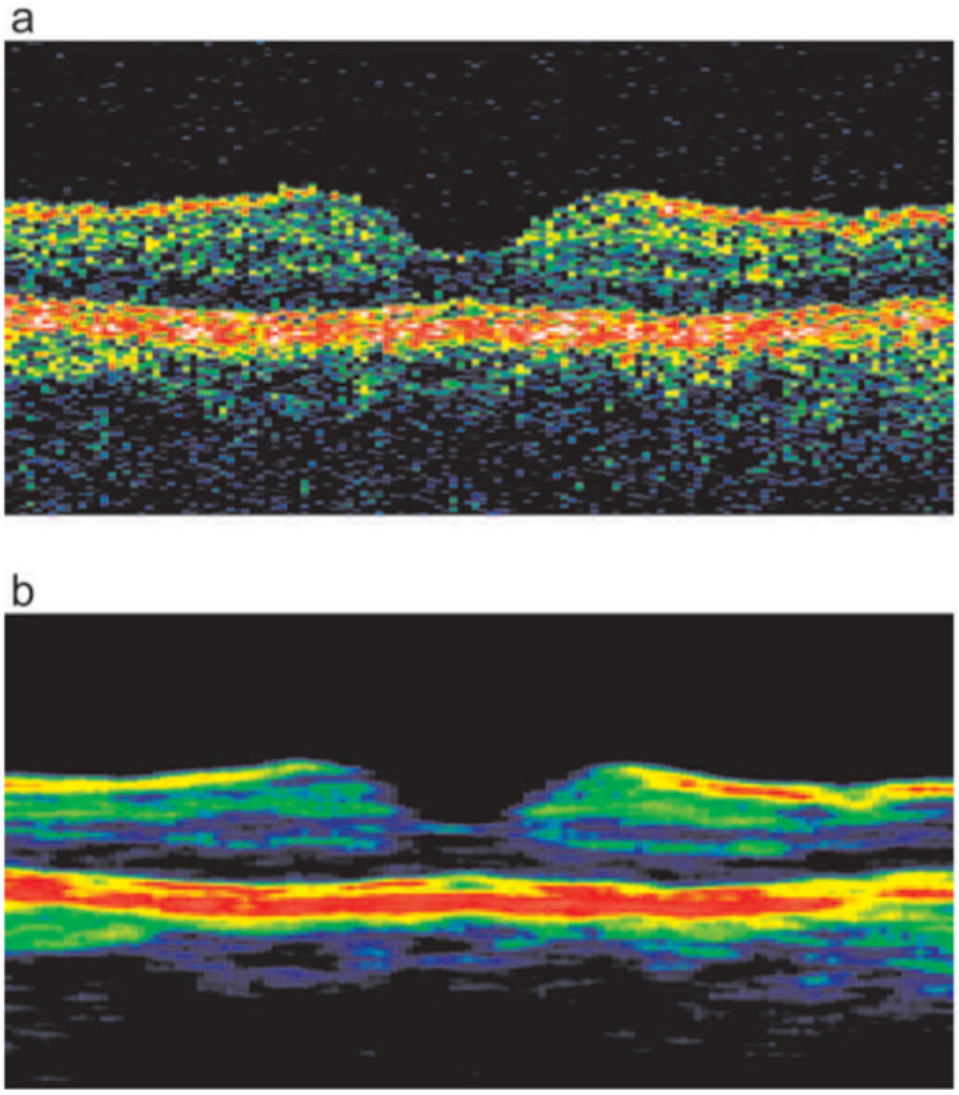

Figure 1.
Preprocessing of the image. (**a**) A raw OCT macular scan image was aligned by cross-correlation. (**b**) A modified mean filter was applied to the aligned image above.

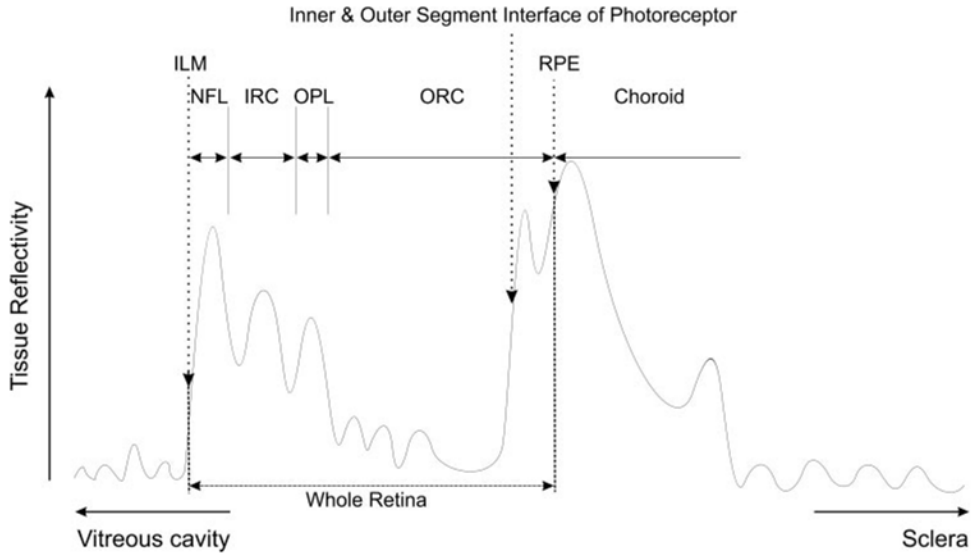

Figure 2.

Segmentation of a sampling line shows a typical sampling line (analogous to an ultrasound A-scan line) plot of tissue reflectivity. The first increase from the noise level was registered as the ILM. The second major peak is RPE complex. The first increase within the RPE complex was the interface between inner and outer segments of the photoreceptors. The RPE was a gap or notch posterior to the interface. Retinal layer structures (NFL, IRC, OPL, and ORC) were defined between the ILM and the interface. The locations of the borders were determined with an adaptive thresholding technique, where cutoff threshold values were calculated based on reflectivity characteristics of each sampling line.

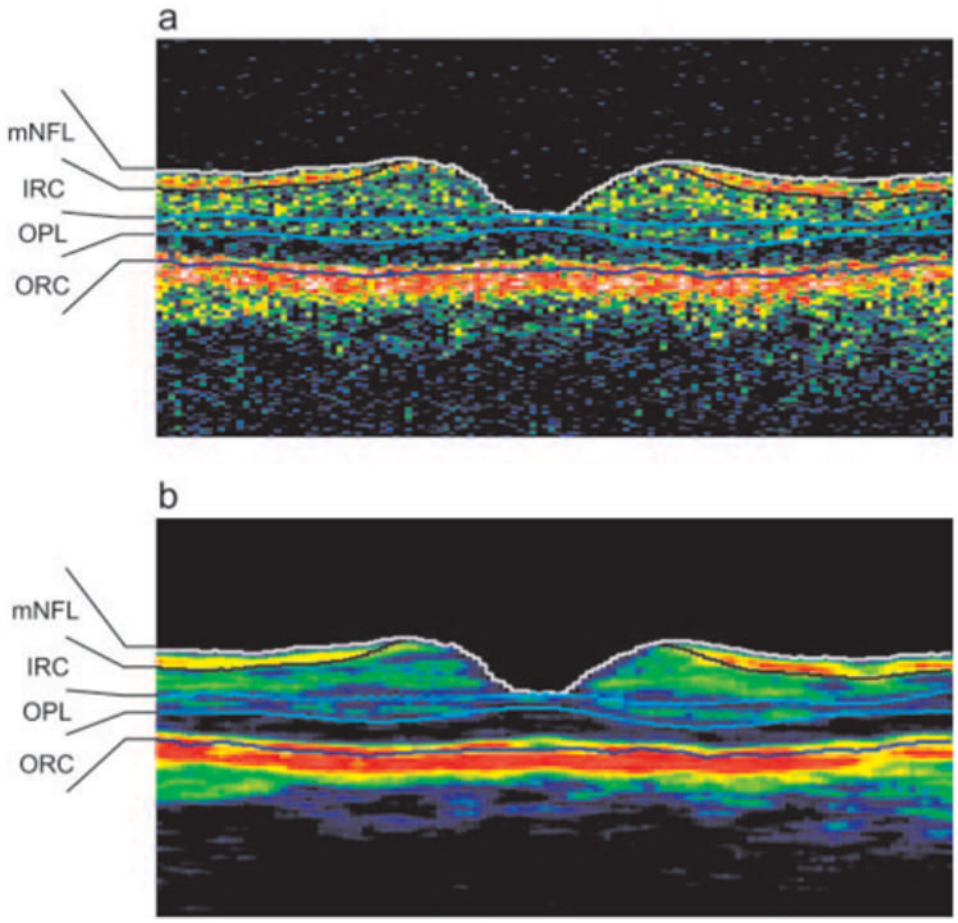

Figure 3.
Macular segmentation analysis sample. (**a**) Detected borders superimposed on the aligned image shown in Figure 1a. (**b**) Detected borders superimposed on the filtered aligned image shown in Figure 1b.

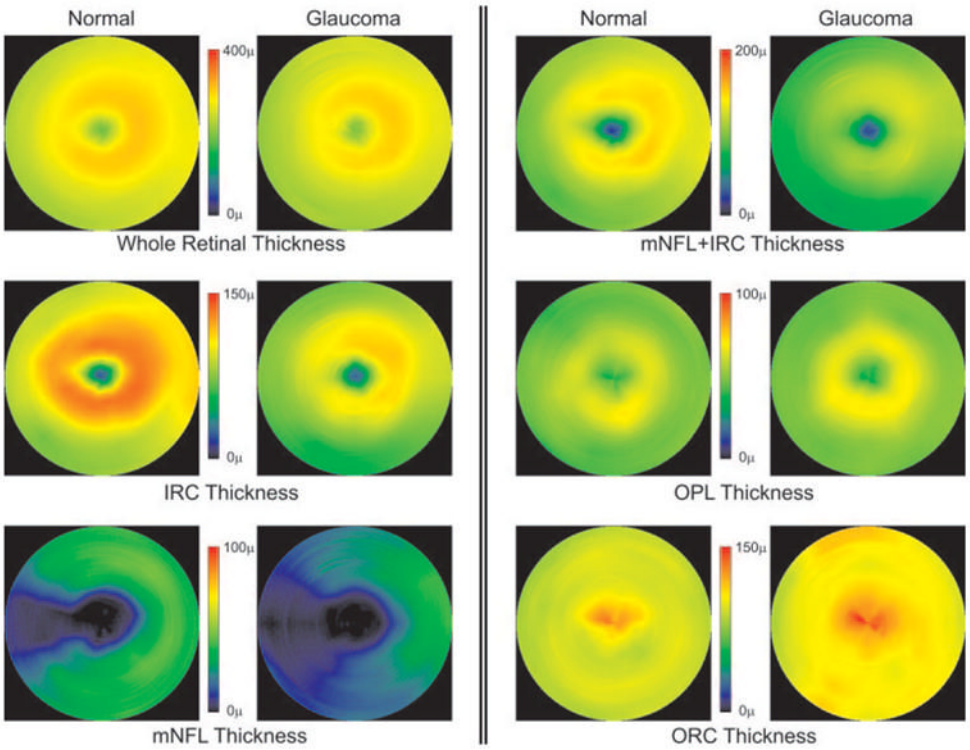

Figure 4.

Comparison of the mean colored maps of each detected layer. Six pairs of mean colored maps, calculated from all 24 normal and 24 glaucomatous eyes, are shown, visually illustrating the quantitative findings. All layers except for the OPL showed statistically significant differences between normal and glaucoma groups. Note that the scale of the color scheme is adjusted for the range of each measured layer.

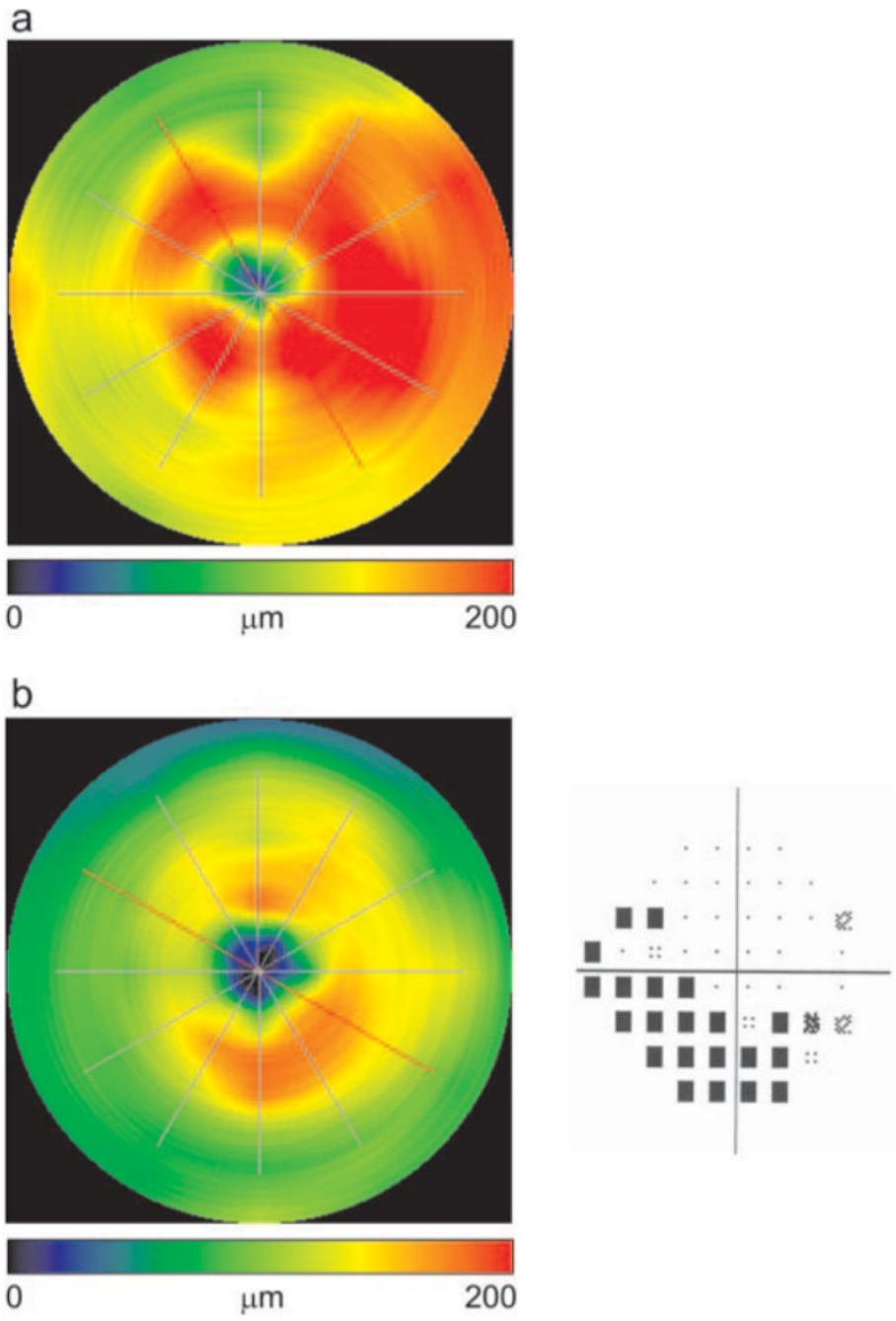

Figure 5.
Color macular segmentation mapping. (**a**) NFL+IRC thickness mapping on a normal eye (OD). A C pattern thickening was clearly seen, where the nasal region was thicker in the papillomacular bundle than the temporal region. Mean NFL+IRC thickness was 123.9 μm. (**b**) NFL+IRC thickness map on a glaucomatous eye (OD) and the corresponding SITA visual field (MD −10.8 dB, PSD 11.3 dB). Superior NFL+IRC thinning was depicted clearly, which agreed with the inferior arcuate visual field defect pattern. Mean NFL+IRC thickness was 99.1 μm.

Table 1

Algorithm Failure

	Expert 1	Expert 2	Both Experts
Good-quality image (288 images of 48 cases)	28 (9.2)	28 (9.2)	31 (10.2)
Poor-quality image (96 images of 16 cases)	41 (50.6)	44 (54.3)	45 (55.6)
Total (384 images of 64 cases)	69 (18.0)	72 (18.8)	76 (19.8)

Data are number of images, with the percentage of the total images in parentheses.

Table 2

Specific Border-Detection Failures

	ILM	NFL	IRC	OPL	RPE
Expert 1	4 (1.0)	13 (3.4)	40 (10.4)	37 (9.6)	12 (3.1)
Expert 2	4 (1.0)	12 (3.1)	40 (10.4)	38 (9.9)	15 (3.9)
Both Experts	4 (1.0)	15 (3.9)	41 (10.7)	39 (10.2)	15 (3.9)

Data are the number of images. Percentages in parentheses were calculated against all images (384 images of 64 cases).

Invest Ophthalmol Vis Sci. Author manuscript; available in PMC 2007 August 2.

Table 3

Mean Thickness Comparison

	Normal (μm) (n = 23)	Glaucoma (μm) (n = 24)	P (Wilcoxon)
mNFL	28.4 ± 4.7	15.6 ± 6.3	<0.0001
IRC	90.7 ± 4.2	73.7 ± 8.8	<0.0001
mNFL + IRC	119.2 ± 6.6	89.2 ± 13.4	<0.0001
OPL	51.0 ± 4.2	49.6 ± 6.7	0.46
ORC	93.8 ± 7.3	100.4 ± 14.3	0.035
Total Retina	265.3 ± 8.3	240.6 ± 23.3	0.0002
cpNFL	93.8 ± 8.8	61.6 ± 17.9	<0.0001

Data are the mean ± SD.

Table 4

Discrimination Analysis: Comparison of AROCs

	mNFL AROC 0.95	**IRC AROC 0.94**	**mNFL + IRC AROC 0.97**	**OPL AROC 0.56**	**ORC AROC 0.68**	**Total Retina AROC 0.82**
IRC AROC 0.94	*P* = 0.83					
mNFL + IRC AROC 0.97	*P* = 0.56	*P* = 0.24				
OPL AROC 0.56	***P* < 0.001**	***P* < 0.001**	***P* < 0.001**			
ORC AROC 0.68	***P* < 0.001**	***P* = 0.009**	***P* < 0.001**	*P* = 0.44		
Total retina AROC 0.82	*P* = 0.09	***P* = 0.04**	***P* = 0.02**	***P* < 0.001**	*P* = 0.27	
cpNFL AROC 0.93	*P* = 0.66	*P* = 0.79	*P* = 0.15	***P* < 0.001**	***P* = 0.01**	***P* = 0.049**

Probabilities were calculated between each pair of AROCs. Significant results are in bold.